CHAPTER III
Results and Discussion

This chapter concerns the first principle study on silicene gas sensors. Based on the DFT calculation, the geometrical structures of of gas molecules adsorbed onto pristine (P) and B/N-doped silicene were determined. The transport properties were calculated using the DFT-based non-equilibrium Green's function (NEGF) theory. This work allows us to investigate the gas detection performance of silicene nanosensors for four different gases. This chapter summarizes the study described in Paper I.

3.1 Geometric and Electronic structures

The geometrical structures of four different molecular gases (NO, NO_2, NH_3 and CO) adsorbed on pristine silicene and doped-silicene nanodevices were relaxed by using DFT [43,44] as implemented in the SIESTA package [49] To describe the weak dispersive interactions, we employed a van der Waals correction [56,57] to the Generalized Gradient Approximation of Perdew, Burke, and Ernzerhof (PBE-GGA) [46] for the exchange-correlation functional in DFT.

A description of van der Waals (vdW) were performed using vdW-DF, as proposed by Dion *et al.* [56]. In this methodology, the exchange-correlation energy is written as

$$E_{xc} = E_x^{GGA} + E_c^{LDA} + E_c^{nl}, \qquad (3.1)$$

where the exchange energy E_x^{GGA} uses the GGA functional, and E_c^{LDA} is the local density approximation (LDA) to correlation energy. The nonlocal correlation-energy part, E_c^{nl}, is defined to include the longest-ranged or most nonlocal energy term which is zero for systems with constant density.

For the ionic relaxation $6 \times 1 \times 4$ *k*-points and for the electronic transport $24 \times 1 \times 1$ *k*-points were used. Furthermore, double-ζ polarized basis sets (DZP) and norm-conserving pseudo potentials [53] were used. The conjugate gradient (CG) method was applied to obtain equilibrium structures with residual forces on atoms below 0.01

eV/$\mathring{A}$. We also employed VASP [code, using the same parameters as in of SIESTA for the relaxation and binding energy calculations with a 400 eV cutoff energy for the plane wave basis and a force tolerance of 0.01 eV/$\mathring{A}$. Silicene has a buckled hexagonal lattice, consisting of 2 Si atoms per unit cell. For transport calculation, each simulated system consisted of $20.57\mathring{A} \times 15\mathring{A} \times 43.54\mathring{A}$ silicene supercell with 132 Si atoms. We use the periodic boundary condition (PBC) along x-direction and z-direction and considerably large supercell to avoid the interaction occurring between mirror images. The neighboring silicene in y-direction was separated by $15\mathring{A}$ of vacuum. Details on supercell construction is presented in Figure 3.1. Silicene has a hexagonal lattice with two atoms per unit cell (A and B) as is shown in Figure 3.1-a. However, is also possible define an unit cell with four atoms and parallepiped shape (see Figure 3.1-b), in which the lattice is characterized by three lattice vectors L_x, L_y and L_z In particular both unit cells are equivalent, but as we are interested in L_z transport properties through the device in certain direction, the parallelepiped unit cell fits better for this application. In all calculation were employed a supercell using a parellepiped unit cell with $3L_x \times L_y \times 11L_z$ and 132 atoms as is shown in Figure 3.1-c. The referred supercell has $20.57\mathring{A} \times 15\mathring{A} \times 43.54\mathring{A}$.

The transport properties were then investigated with the TranSiesta code [58], combining the NEGF method and DFT. This was done to perform electronic transport calculations in order to visualize the degree of capability of pristine silicene and doped-silicene nanodevices as an electric nanosensors to distinguish four different molecular gases (NO, NO_2, NH_3, and CO). The basis sets and the real-space grid employed in the transport calculations are identical to those described above for the geometrical optimization part. The system was divided into three parts: two leads (left and right) and a scattering region in between them. The left panel of Figure 3.2 shows upper (pristine) and lower panel (doped) hexagonal 2D silicene that was used as a molecular gas sensor. The red shaded rectangles represent the electrodes or leads (left/right) and the region in between was the scattering region. Nitrogen (N) and boron (B) are the two substituted atoms used to functionalize silicene.

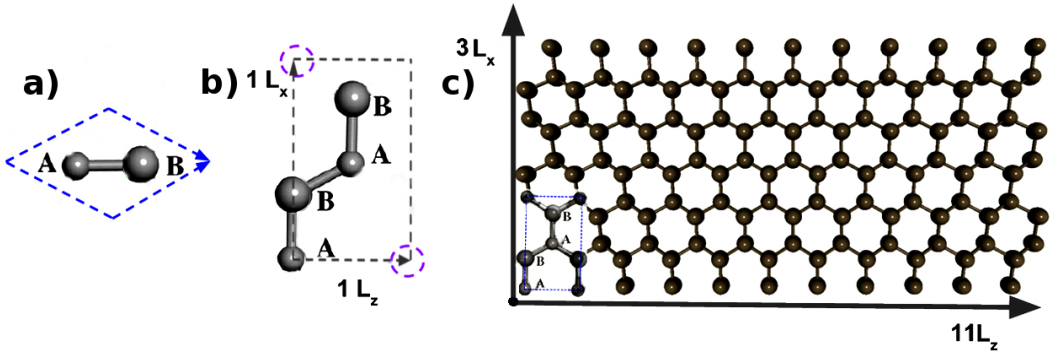

Figure 3.1: a) Hexagonal 2D lattice with two atoms per unit cell for silicene; b) A parallelepiped unit cell with four atoms per unit cell and (c) supercell used in relaxations and also transport calculation.

Defining the boundary as a region, where the charge density matches with the bulk electrodes and using localized basis sets, the NEGF for the scattering region $\mathcal{G}(E,V)$ can be formulated as following:

$$\mathcal{G}(E,V) = [E \times S_{\mathrm{S}} - H_{\mathrm{S}}[\rho] - \Sigma_{\mathrm{L}}(E,V) - \Sigma_{\mathrm{R}}(E,V)]^{-1}$$

where S_S and H_S are the overlap matrix and the Hamiltonian, respectively, for the scattering region. $\Sigma_{L/R}$ are self-energies that account for the effect from the left (L) and right (R) electrodes upon the central region. The self energies are given by, $\Sigma_\alpha = V_{S\alpha} g_\alpha V_{\alpha S}$, where g_α are the surface Green's functions for the semi-infinite leads and $V_{\alpha S} = V_{S\alpha}^\dagger$ are the coupling matrix elements between the electrodes and the scattering region. The Hamiltonians can be calculated through several approaches (e.g., using tight-binding methods). Actually, H_S is a functional of electronic density and for this reason, we used the Hamiltonian obtained from the DFT calculations. The charge density is self-consistently calculated via Green's functions until convergence is achieved; the transmission coefficient $T(E)$ can be obtained as:

$$T(E) = \Gamma_{\mathrm{L}}(E,V)\,\mathcal{G}(E,V)\,\Gamma_{\mathrm{R}}(E,V)\,\mathcal{G}^{\dagger}(E,V)$$

where the coupling matrices are given by $\Gamma_\alpha = i\left[\Sigma_\alpha - \Sigma_\alpha^\dagger\right]$, with $\alpha \equiv \{\mathrm{L},\mathrm{R}\}$. Further details regarding the methods for calculating electronic transport properties can be found in the literatures [51,58].

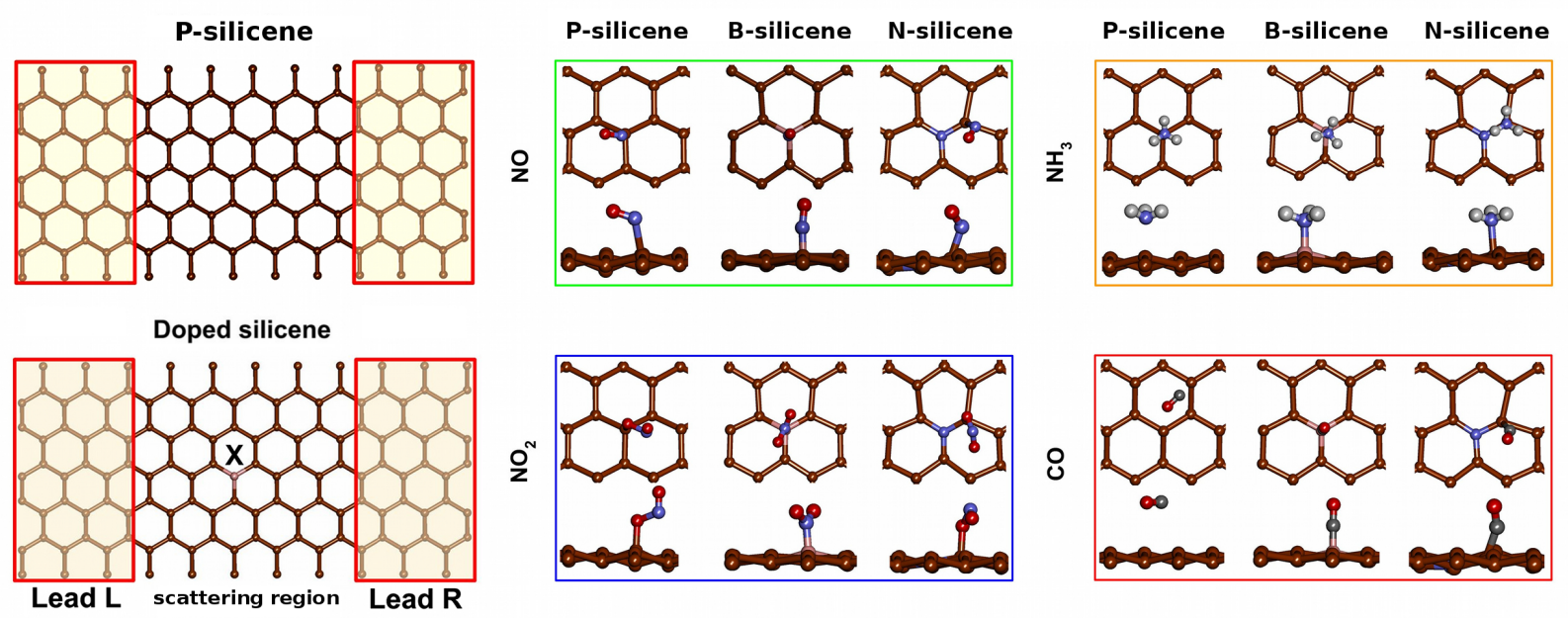

Figure 3.2: The device setup is shown in the left panel for pristine (upper) and doped silicene (lower) where X marks the site for B and N doping. The central and right panels show the most stable congurations for the four gas species NO, NH_3, NO_2 and CO when adsorbed on either pristine, B-doped or N-doped silicene.

Figure 3.2 shows a schematic device setup for P- and (B and N) doped-silicene used for gas detection. First, we address the structural stability of molecular adsorption geometries by initially placing each molecule on P- and B/N- silicene, respectively. Figure 3.3 shows four possible adsorption sites of gases on the P-silicene. They are referred to as the (I) hill, (II) valley, (III) bridge, and (IV) hollow sites. For doped sensors (B and N), only the gas adsorption above the B and N atoms and their nearest neighbors were tested. For these positions, different molecular orientations were examined. For diatomic gases (CO and NO), we investigated three possible orientations. Their molecular axis was oriented parallel and perpendicular (with the O pointing up and down) with respect to the silicene surface. For tri- and tetra- atomic gases (NO_2 and NH_3), two orientations were tested, i.e., one with the N atom pointing to the surface and the other with the N atom pointing away from the surface.

For P-silicene, twelve starting configurations for CO and NO (diatomic gases) and eight for NO_2 and NH_3 (tri-/tetra- atomic gases) were considered. Note that the starting configuration was not the final one. We sometimes see energy degenerated structures with very small binding energy differences. CO has two degenerate adsorption configurations, i.e., III-3 and IV-3. NO exhibits two most stable configurations, i.e., II-2 and III-2. NH_3 presents two degenerate adsorption configurations, i.e, IV-1 and II-1. The most stable configurations including its binding energy and binding distance are presented in Figure 3.2.

For P-silicene, in principle, there is no favorable site to adsorb the molecular gas. The interaction of NH_3 and CO with P-silicene is mostly of van der Waals type, whereas NO and NO_2 exhibit covalent chemisorption bonding. For doped devices, the gas molecules energetically prefer to be chemisorbed on the top of a B atom for B-silicene and chemisorbed on the top of a Si atom nearest to the N dopant for N-silicene. The binding energies of doped-silicene become larger than that of pristine, and the binding distances between the gases and doped-devices are shortened (see Table 3.1) as expected.

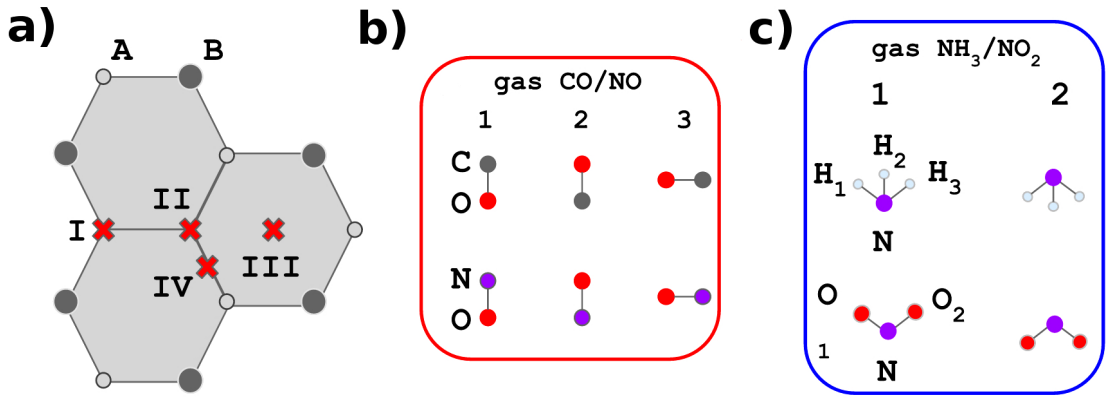

Figure 3.3: (a) Possible adsorption sites of gases on the hexagonal lattice of P-silicene: (I) hill, (II) valley, (III) bridge, and (IV) hollow sites. Different molecular orientations were examined for (b) CO and NO (diatomic gas molecules) with three possible orientations and (c) NH_3, and NO_2 (tri- and tetra-atomic gas molecules) with two initial orientations.

For doped-silicene, we examined only the gas adsorption above the dopants and their nearest neighbors since these adsorption sites are the most active. As shown in the main manuscript, we observed that different gases exhibit distinct configurations for each doped-silicene device. CO and NO (diatomic gases) binding with the doped-silicene at the C and N atom, respectively. They were tilted with respect to the surface for N- silicene, but aligned perpendicularly for B-silicene. NH_3 bonds to the silicene with its N atom for both doped-devices. NO_2 bonds to B-silicene with its N atom (B-N bond) and to N-silicene with an O atom (Si--O bond).

To better understand the binding strength of gas adsorption, we analyzed the charge density of three nanosensors, i.e. pristine and with the two dopants, as shown in Figure 3.4. The pristine device was considered a neutral device, in which the charge density is equally distributed through the device. Although the doped nanodevices were also neutral, they had charge localization in the vicinity of each dopant that led to the conclusion that atoms had electron donor and acceptor characteristics for B and N dopants, respectively. We furthermore considered the electronegativity of all species involved in the devices. For B-silicene, the charge is concentrated close to B (it became slightly negative) and the three nearest-neighbor Si partially share this charge. The second device doped with N has higher charge accumulation close to N, compared to the former case, and the neighbor Si atoms become less charged. These facts are due to the electronegativity hierarchy of Si and dopant atoms; (N < B < Si). N has a tendency to attract electrons more strongly than B and Si. Figure 3.4 confirms this assumption

that the charge was localized on the dopant for N-silicene and spread up the bonds for the B-silicene system.

Table 3.1: Calculated binding energy E_b , binding distance (D) and charge transfer from the silicene to molecules $\Delta Q(|e|)$

devices	gas	E_b (eV)	D (Å)	$\Delta Q(\|e\|)$
P-Silicene	NO	-0.73	2.11	0.19
	NO_2	-1.30	1.77	0.37
	NH_3	-0.26	2.27	0.16
	CO	-0.10	3.24	-0.03
B-Silicene	NO	-1.01	1.46	0.19
	NO_2	-3.02	1.50	0.08
	NH_3	-0.80	1.63	0.49
	CO	-1.19	1.51	0.32
N-Silicene	NO	-1.95	1.87	0.01
	NO_2	-3.50	1.76	-0.06
	NH_3	-0.80	2.06	0.42
	CO	-0.99	1.88	0.20

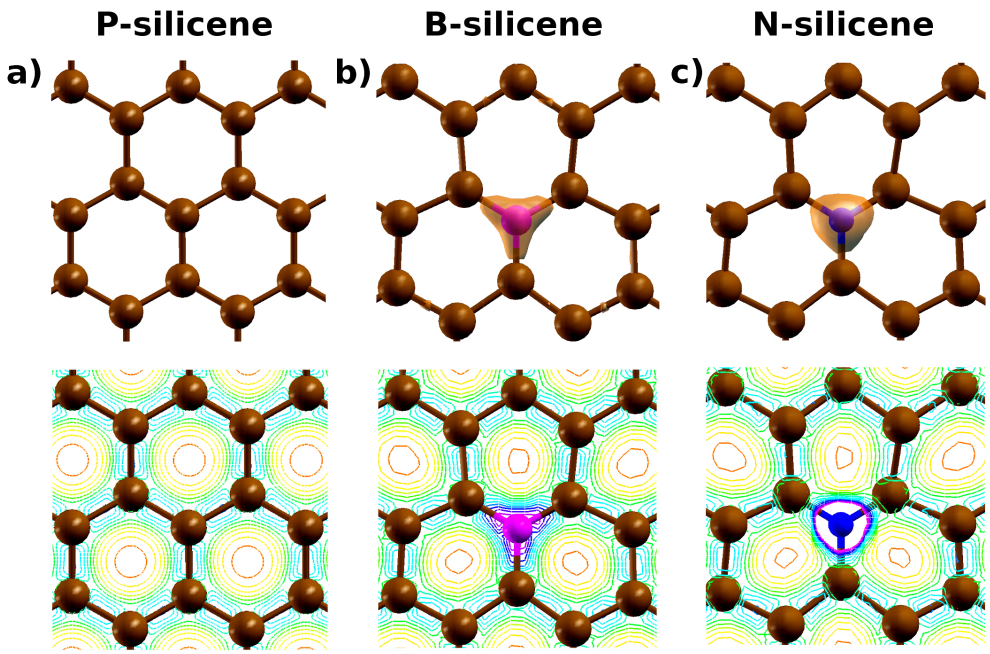

Figure 3.4: Charge density for (a) pristine silicene; (b) B-doped silicene and (c) N-doped silicene. The plotted isosurface corresponds to a value of 0.08$e \times bohr^{-3}$ for all panels.

The binding sites and molecular orientations of adsorbed gases on the nanosensor devices (Figure 3.2) needs to be discussed in more detail. For example, NO with an odd number of valence electrons has one unpaired electron on N atom which makes it highly reactive. As a result, NO always binds to the pristine silicene with N atom (see panel NO in center of Figure 3.2). As the second case in point, NH_3 has a tendency to bind to the pristine system with N, while the three H atoms point up. This is the simplest case because NH_3 has a lone pair on a N atom. The interesting case is for N-silicene, both dopant and gas have N atoms with the same electronegativity. Consequently, the NH_3 prefer binding with one Si atom close to a N atom (see Figure 3.2). Comparing the adsorption of NH_3, NO and NO_2 on P-silicene with previously reported results [37], our calculated binding energies are seen to differ in general by less than approximately 18%, however, the disagreement is larger for NH_3. When compared to the binding energy and the charge transfer of NH_3 on P-silicene in Ref. 61, our results agree quite well; there is a difference of 28.8% for binding energy and the value of charge transfer is exactly the same. The variation in results could be due to the difference of localized basis and plane-wave basis as well as the difference of dispersion correction. Additionally, our results are found to be in good agreement with

a previous DFT study \cite{Feng:2014ip} except for the cases of physisorbed gases, i.e., CO and NH_3. The binding energy difference between those results and ours for NH_3 amounts to almost 60%. This large discrepancy stems from the inclusion of the long-range van der Waals (vdW) interactions in our present work. Furthermore, we systematically optimized the adsorption geometry of each gas molecule considering various possible molecular orientations and adsorption sites as a starting point for each relaxation. Overall, we find qualitatively good agreement with previous studies for the most stable configuration of the adsorbate on P-silicene. However, when the device is doped, the gas prefers binding to the devices with a C atom. Finally, for NO_2 on P- and N-silicene devices, a covalent bond is formed between the Si atom and O atom due to the existence of an unpaired electron on one of the O atoms. For B-silicene, it is more energetically favorable that NO_2 binds to the system with its N atom. This results from the coordinate covalent bond in which an electron pair on the N atom enter to a vacant p-orbital on the B atom.

3.2 Possibility of Silicene Device as a Gas Sensor

Two of the most important challenges to build a good commercial sensor are the ability to detect different harmful gases (selectivity) and to improve the ability to sense some gas molecules (sensitivity). Experimentally, one of the most important parameters for sensing a gas is usually a variation in resistance or conductance, known as sensitivity. This property can be defined as $S(\%) = \frac{|G - G_0|}{G_0}$, where G and G_0 are the zero bias conductance for nanosensor with and without gas, respectively. Here, the conductance was simply calculated as $G = G_0 T(E_F)$, where $G = G_0 T(E_F)$ is the quantum conductance, e is the charge of the electron and h is Planck's constant.

The transmittance $T(E)$ of the P-, B- and N- silicene devices is presented in Figure 3.5-(a),(b),(c), respectively. Obviously, the gas adsorption significantly affects the $T(E)$of the three devices. For example, the adsorption of NO and NO_2 on P-silicene results in a remarkable decrease of the $T(E)$, whereas for CO and NH_3 the changes are not very pronounced. Additionally, the results indicate that doping either B or N atoms into silicene improves the detection of CO and NH_3, compared to that of P-silicene. Without the presence of gas, the $T(E)$ of doped-silicene was lower than that of the P-silicene (as depicted by the black dashed line in Figure 3.5. The $T(E)$ of B-silicene was lower than that of N-silicene. It was shown that the gas adsorption on the B-silicene device affected the $T(E)$, but not as strongly as for N-silicene.

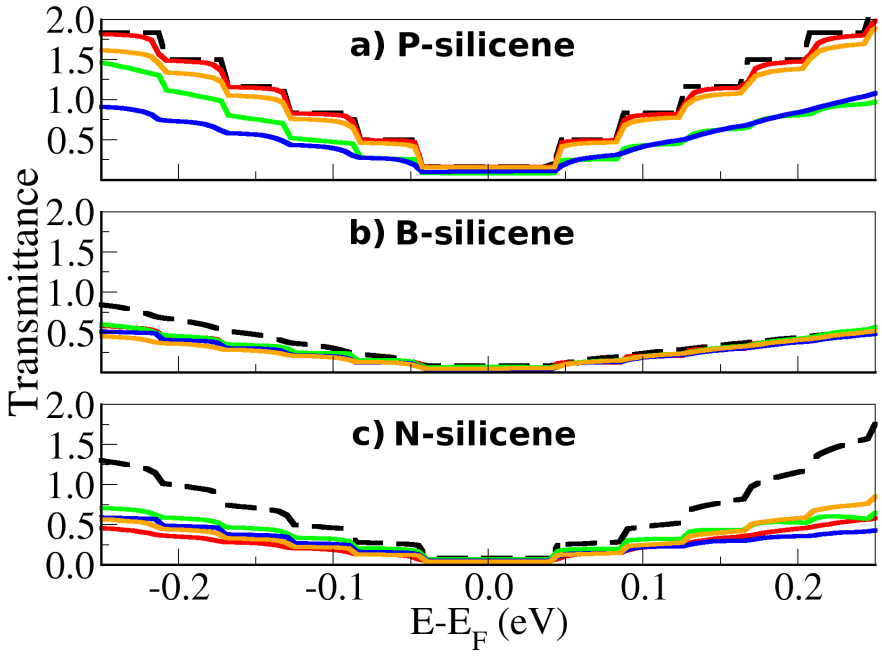

Figure 3.5: Transmittance as a function of energy, where the Fermi energy (E_F) is set at zero, is shown for (a) P-silicene; (b) B-silicene and (c) N-silicene. Red, green, orange and blue lines represent the transmittance for CO, NO, NH_3 and NO_2 adsorbed on the devices, respectively, while black dashed lines represent that of the reference system (P-,B- and N-silicene devices without gas).

Fig. 3.6-a presents the sensitivity as a function of binding energy of the three devices (P-, B-, and N- silicene) for NO, NO_2, NH_3 and CO gas molecules. In order to evaluate whether silicene and doped silicene can be good gas nanosensors, we should have both high and distinct sensitivities when the sensor is exposed to different gases. Another important aspect is about how long the gas can stay on the device. This is the translocation time τ and it is proportional to $\approx \exp\left(\frac{-E_b}{k_B T}\right)$,where E_b is binding energy, k_B is the Boltzmann constant and T is temperature. We expect small binding energies to lead to fast desorption of gases from the devices. Analyzing Figure 3.6-a, we found that the binding energies were generally less than 2 eV. The only exception occurred for NO_2 on the doped-devices ($E_b > 3$ eV). Turning our focus to each device, we observed that the P-silicene device (see Figure 3.6-b) has binding energies range from -0.1 to -1.3 eV and their respective sensitivities were strongly dependent on gas molecules. The sensitivity of the P-silicene device increased linearly with increasing binding energy. The sensitivities were found to follow an ascending order, i.e., CO < NH_3 < NO < NO_2. However, CO and NH_3 have low sensitivity. Spin-polarized calculations were also performed, but the resulting energy differences are smaller than the thermal

fluctuations at the envisioned operating temperature of the sensor, namely room temperature ($k_BT \approx 0.025$ eV). In a test, we found that the transmittance for each channel (up and down) exhibits only minor quantitative differences which do not affect our conclusions. For these reasons, spin polarization effects were neglected in our study.

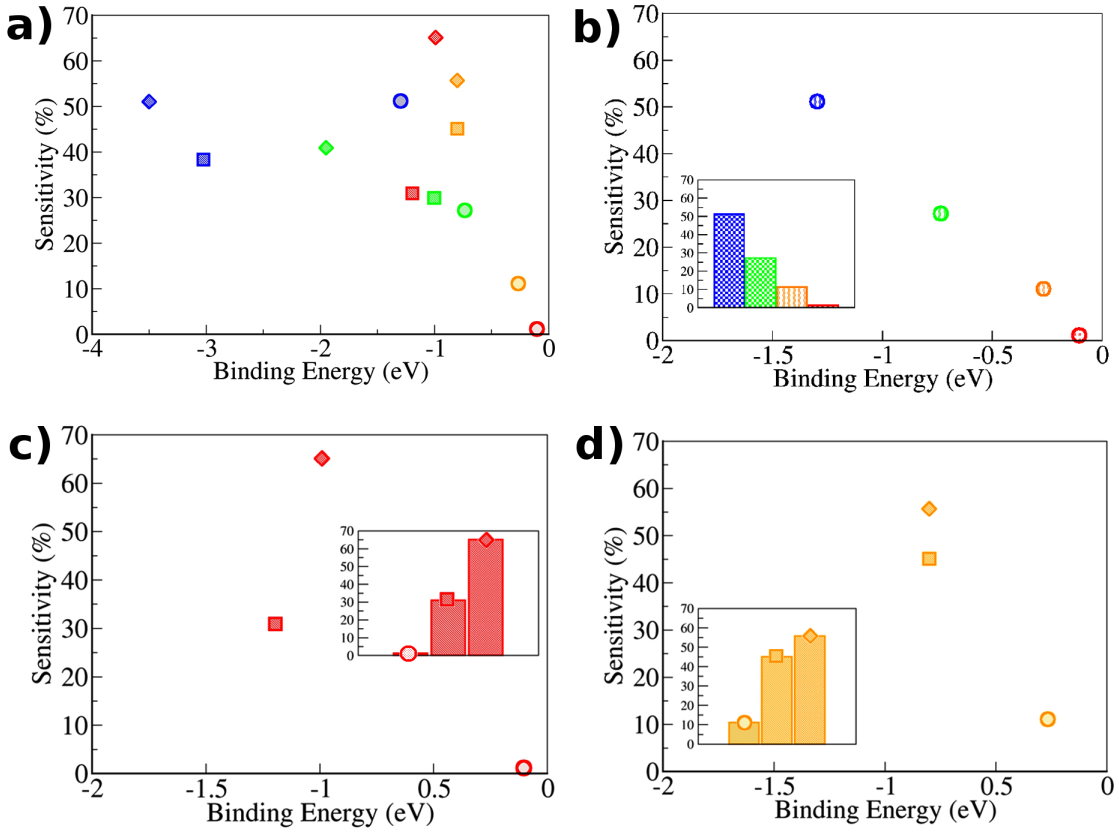

Figure 3.6 (a) Sensitivity versus binding energy for NO (green), NO_2 (blue), NH_3 (orange) and CO (red) gas molecules on P-silicene (circle), B-silicene (square) and N-silicene (diamond) devices, respectively; (b) the four gas species on P-siliene (the inset shows the sensitivity comparison for P-silicene); (c) CO on three devices and (d) NH_3 on three devices. The insets of (c) and (d) are the sensitivity comparison for one gas on the three different devices.

Next, we will address how to improve the sensitivity of these gases. As can be seen in Figure 3.5-a, by the introduction of dopant atoms, N-silicene (diamond shape) and B-silicene (square shape) exhibited higher binding energies and subsequently sensitivity.

This is especially true for CO and NH_3 (see Figure 3.6-c and 3.6-d). Better sensitivity was obtained due to increased binding energies (see Table 1). Interestingly, CO molecules can distinguish p-type and n-type doping of silicene (see Figure 3.5-c). This contradicts the findings of a previous study of a graphene-based gas sensor [60]. The CO on N-doped silicene showed a sensitivity around two orders of magnitude higher than that of CO on B-doped silicene. To explain why the sensitivity increased substantially for these molecular gases, the charge transfer of these systems will be investigated.

The transport properties of silicene devices relate to the change in local charge distribution around the B and N impurity atoms as a consequence of the charge transfer from gas molecules adsorbed on silicene. To visualize the charge transfer of NH_3 and CO adsorbed on the devices, we calculate the charge density difference: $\Delta\rho(\vec{r}) = \rho_{device+gas}(\vec{r}) - (\rho_{device}(\vec{r}) + \rho_{gas}(\vec{r}))$, as presented in Figure 3.7. The contour plot of $\Delta\rho$ illustrates the charge accumulation/depletion in the system, i.e., we can quantitatively describe the idea of the charge transfer. For doped silicene, there is charge accumulation indicating the hybridization of orbitals at the nanosensor surface in which NH_3 and CO is adsorbed (see Figure 3.7). Such orbital hybridization is absent for physisorption of the gases on P-silicene. In other words, the charge-transfer capability increases with the increasing bonding charge densities.

Furthermore, we investigated the electron charge transfer using the Mulliken population analysis (see Table 1). It is notable that the positive charge transfer occurred from the gas molecules to the silicene. As discussed above, our results reveal the difference in charge redistribution of three nanosensors (see Figure 3.7). For B-silicene, as shown in Table 1 all gases examined in the current study act as donors. They donate charges to the device, resulting from the vacant p-orbital on the B atom. A large amount of charge transfer is obtained, especially for NH_3, which is electron-donating molecule. For N-silicene, the electron-rich gas molecules prefer to adsorb on the top of one positively charged Si close to N (see Figure 3.2). A negative charge transfer value as observed only for NO_2 due to its strong electron-withdrawing capabilities.

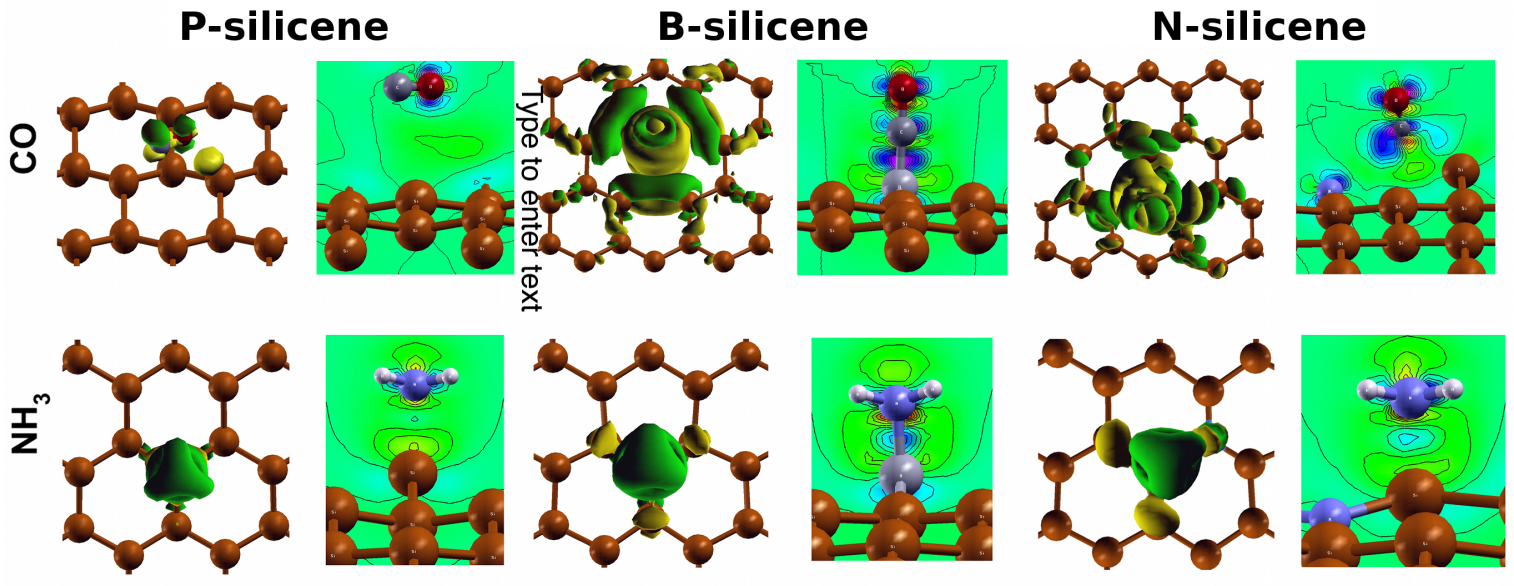

Figure 3.7: Charge density difference for CO (upper) and NH_3 (lower panel) on P-, B-, and N-silicene devices for each type of nanosensor. Isosurfaces are plotted for isovalues of 0.0004 (0.002) $e \times bohr^{-3}$ for CO (NH_3) alongside contour plots. For the isosurface plots, green color represents negative charge density difference while yellow corresponds to a positive change in charge density.

A few important aspects should also be discussed. The first is the influence of substrates on gas sensing performance. According to the experimental studies, for all the cases, silicene was synthesized on top of some substrates [14,22,23,25]. A very recent study [36] elaborated the effect of Ag(111) substrate on the electronic structures of gas molecules on silicene, indicating a slight increase in adsorption energies and charge transfer. We expected that the conductance could be changed due to the influence of different substrates, changing the sensitivity, but the interaction between silicene should not substantially change the overall trend with this additional component. The second point is about the experimental challenge to control the doping in silicene. Recent experimental studies reported on potassium adsorption in silicene [62], inducing n-type doping. Additionally, a theoretical study also showed the stability of B/N substituted doping into silicene [63]. Therefore, if reactive centers can be created as we have shown, their gas sensing performance will be improved enormously. In addition, there remain many challenging problems. For instance, a recent study [64] demonstrated the dissociative adsorption of molecules (H_2, O_2, CO, H_2O and OH) on defect sites in graphene and silicene. In our study, these molecules remain intact on silicene, but certain molecules may dissociate due to increased chemical reactivity at the defect sites as it has been reported previously [62].